Available online at www.sciencedirect.com

ScienceDirect

Physics Procedia 87 (2016) 61 – 71

Physics Procedia

44th Annual Symposium of the Ultrasonic Industry Association, UIA 44th Symposium, 20-22 April 2015, Washington, DC, USA and of the 45th Annual Symposium of the Ultrasonic Industry Association, UIA 45th Symposium, 4-6 April 2016, Seattle, WA, USA

Ultrasonically-assisted polymer molding: an evaluation

Matthew Moles[a*], Anish Roy[a], Vadim Silberschmidt[a]*

[a]*Wolfson School of Mechanical, Electrical and Manufacturing Engineering, Loughborough University, Epinal Way, Loughborough, Leics LE11 3TU, United Kingdom*

Abstract

Energy reduction in extrusion and injection molding processes can be achieved by the introduction of ultrasonic energy. Polymer flow can be enhanced on application of ultrasonic vibration, which can reduce the thermal and pressure input requirements to produce the same molding; higher productivity may also be achieved. In this paper, a design of an ultrasound–assisted injection mold machine is explored. An extrusion-die design was augmented with a commercial 1.5 kW ultrasonic transducer and sonotrode designed to resonate close to 20 kHz with up to 100 µm vibration amplitude. The design was evaluated with modal and thermal analysis using finite-element analysis software. The use of numerical techniques, including computational fluid dynamics, fluid-structure interaction and coupled Lagrangian-Eulerian method, to predict the effect of ultrasound on polymer flow was considered. A sonotrode design utilizing ceramic to enhance thermal isolation was also explored.

Keywords: ultrasound; polymer; melt; processing; finite element; thermal isolation

1. Introduction

Polymer processing is an important and diverse field in the manufacturing industry. By applying vibration to a polymer flow, for example as reviewed in Ibar (1998), its effective flow rate may be enhanced. It is generally believed that the observed improvements are due to one, or a combination, of three possible modes: (1) high shear rate imposed by the vibrating surface that reduces the viscosity of the polymer melt; (2) shearing of polymer chains

* Corresponding author. Tel.: +44 1509 227614.
E-mail address: m.moles@lboro.ac.uk

doi:10.1016/j.phpro.2016.12.011

at the molecular level that reduces the effective molecular weight; and (3) rapid oscillation of the polymer molecules that induces localized heating.

In this paper some critical aspects of the application of ultrasound (US) to polymer processing are considered. First, the design of a commercial transducer and sonotrode were evaluated for the potential application of ultrasonically-assisted injection molding. The design concept is based on a patented technique (WO 2004/024415 A1). Essentially, the polymer passes through a die, where it is exposed to an ultrasonic energy field before continuing to the mold. An interstitial die, located between the extruder and the injection mold die, was designed. The US application targets increased cost, improving effectiveness due to reduction in thermal and/or pressure requirements. The application of fluid-dynamics techniques to establish US interaction with the polymer melt was then explored. Next, a method of enhancing the thermal isolation of US equipment for polymer melt processing is presented. The goal was to ensure the US device did not suffer from exposure to high temperatures, typical of molding machines.

Nomenclature

BC	boundary condition
CFD	computational fluid dynamics
dt	time increment
f	frequency
FEM	finite-element modeling
FSI	fluid-structure interaction
US	ultrasound

2. Method

2.1. Simulation methods

2.1.1. Finite-element modeling: solid mechanics

To study and optimize an ultrasonically-assisted polymer molding process, finite-element modeling (FEM) was performed in a commercially software (Abaqus, version 6.14). Material properties were as specified in Table 1. All models were full 3D representations, without symmetry, using the C3D8R hex elements or C3D8RT element type for thermal analysis. Dimensions of the commercial sonotrode and interstitial die were provided by our partners. A schematic diagram of the in-house designed thermally isolated die is shown in Figure 1. Modal analysis used the linear perturbation frequency step, with bounds of 15 kHz and 25 kHz.

The effect of pressure loading on the sonotrode's tip in the interstitial die as a result of exposure to the fluid flow was evaluated by applying a pressure load to the appropriate region of the tip.

Thermal analysis was transient until steady-state, with thermal input via heaters as per the design specification. The atmosphere was considered to be 297 K. For the interstitial die, the shared boundaries with an extruder and a mold were 473 K and 323 K, respectively; the heater set point was 473 K. For the in-house designed thermally isolated transducer the set point was 423 K.

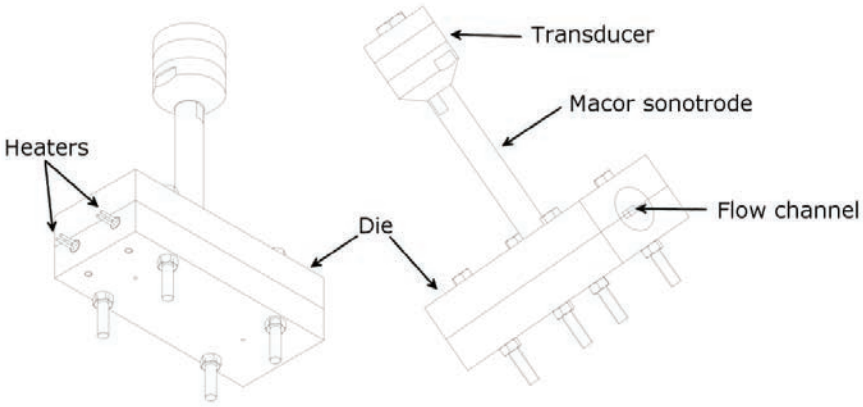

Figure 1. Schematic diagram of the in-house designed die and thermally isolated transducer.

Table 1. Material properties specified for FEM.

Material	Density ($kg.m^{-3}$)	Elastic modulus (GPa)	Poisson's ratio (unitless)	Coefficient of thermal expansion ($m.m^{-1}.K^{-1}$)	Thermal conductivity ($W.m^{-1}.K^{-1}$)	Specific heat capacity ($J.kg^{-1}.K^{-1}$)	Emissivity ($W.m^{-2}$)	Heat transfer coefficient to air ($W.m^{-2}.K^{-1}$)
Aluminum, 6082	2700	70	0.33	2.31E-5	180.0	894	0.05	4.8
Brass	8470	105	0.34	2.03E-5	116.0	380	0.1	-
Macor	2520	66.9	0.29	9.3E-6	1.46	790	0.9	2.5
NCE40 piezoceramic	7750	Manufacturer's orthotropic data	0.36	4.0E-6	2.0	480	0.9	2.5
Steel, P20 tool	7850	205	0.30	1.28E-5	34.0	460	0.79	7.9
Titanium, grade 2	4510	105	0.37	9.20E-6	16.4	560	0.2	5.0

2.1.2. Finite element modeling: fluid dynamics

Fluid dynamics analysis was also performed in Abaqus using three techniques: computational fluid dynamics (CFD), fluid-structure interaction (FSI) and a coupled Eulerian-Lagrangian (CEL) scheme. The Cross viscosity model was used in the CFD solver, while the Cross-Williams-Landel-Ferry model (Eq. 1) from Mueller and Henning (2015) was implemented as a VUVISCOSITY for CEL:

$$\eta = \eta_\infty + (\eta_0 - \eta_\infty)\frac{1}{1+(\frac{\eta_0\dot{\gamma}}{\tau^*})^{1-n}} \tag{1}$$

In this equation the melt viscosity η is defined using the viscosity at high η_∞ and low η_0 shear rates $\dot{\gamma}$. Power-law behavior is defined by n, while the transition from Newtonian to shear thinning behavior is governed by τ^*. The explicit solver also requires an equation of state (EOS) model for which the Tait model, also from Mueller and Henning (2015), was implemented using VUEOS:

$$\frac{dp}{d\rho} = b_3 \times \exp(b_4(T - b_5))\left(\frac{b_1 + b_2(T - b_5)}{C}\right) \tag{2}$$

$$\frac{dp}{dE} = \frac{-b_4}{c_w} b_3 \times \exp(b_4(T - b_5))(\exp\left(\frac{\rho}{C}(b_1 + b_2(T - b_5)\right) - 1) \tag{3}$$

Equations 2 and 3 define the pressure-density and the pressure-energy differentials, respectively. The two equations utilize temperature T and heat capacity C, and a number of material specific constants (b_1-b_5) obtained from data fitting. The user routines implemented for CEL permit the use of temperature as a variable, whereas the default Abaqus implementation permits only definition of parameter sets for discrete temperatures. Experimental fitted data from Wang et al. (2009), as shown in Table 2, was used for the viscosity models. Similar rheological behavior is produced by the two viscosity models as shown in Figure 2.

In the CFD and FSI simulations the flow domain was described as a cylinder with the sonotrode oriented perpendicular to the flow; the outlet converged to a small diameter. Boundary conditions were defined at the inlet with a velocity of 0.5 m.s^{-1}, and at the outlet as zero pressure while the walls were defined as no slip.

Table 2. Fluid model parameters for polypropylene.

FEM	Model	η_0	η_∞	λ	n	τ
CEL	Cross-Williams-Landel-Ferry	1.24E6	2	-	0.2065	57681
CFD/FSI	Cross	223	1.5	8.52E-3	0.14	-

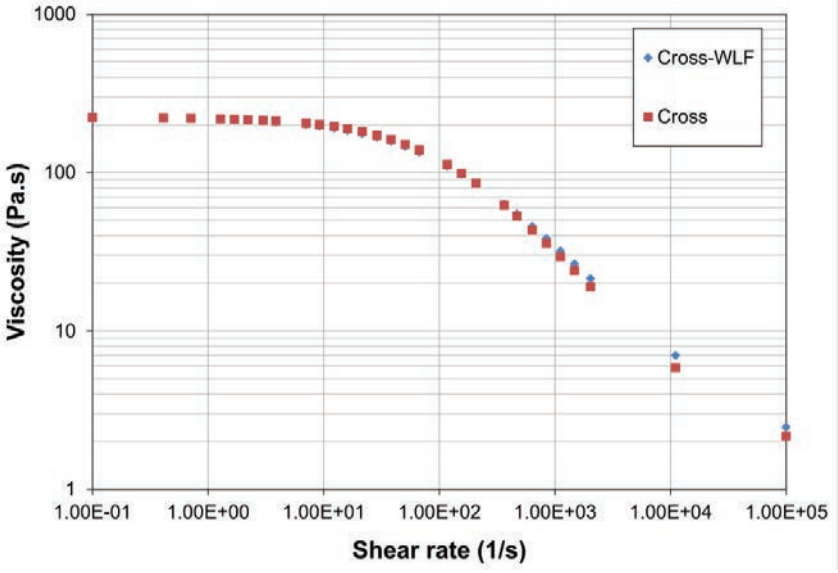

Figure 2. Rheological viscosity models used in FEA fluid flow simulations.

2.2. Experimental methods

2.2.1. Manufacture of the thermally isolated transducer

An US transducer designed and built in-house utilizing a machinable-ceramic (Macor; Corning Inc.) sonotrode and NCE40 piezoceramics (Noliac A/S) was tested. The back mass was made of mild steel and the front mass of aluminum alloy 6082. Using a torque wrench a bolt load of approximately 28.3 kN was applied to give a 28 MPa pressure on the piezoceramics. The device was coupled to an aluminum polymer melt die, with a rectangular-section melt channel, using a steel grub screw. Two 400 W cartridge heaters were located in the rear die; power was controlled by a Eurotherm controller and K-type thermocouple embedded in center of the die. The transducer and die are shown in Figure 1.

2.2.2. Evaluation of the thermally isolated transducer

Thermal imaging of the system was performed using an infra-red camera (Micro-Epsilon TIM480). Stickers of known emissivity were placed on the device's surface.

Transducers under test were driven by a 250 W (rated at 4 Ω load) power amplifier and sine wave from a signal generator (Agilent 33210). Displacement of the transducer due to US was quantified using a laser vibrometer (Polytec OFV 3001). Measurements were made with the laser head oriented perpendicular to the surface.

In order to evaluate flow enhancement, initial tests used dry sharp sand at room temperature. The die was packed with sand, then the time taken for the die to empty was compared with and without US.

3. Results and discussion

3.1. Interstitial die for injection molding

Simulation results are presented here for the design evaluation of the US-assisted injection molding interstitial die. The effect of service conditions on the resonance mode were considered, then the thermal risk to the piezoceramics was assessed. Finally, fluid dynamics approaches using Abaqus for the prediction of the polymer melt interaction with an ultrasonic device are considered.

3.1.1. Modal analysis

The transducer manufacturer quoted a 20 kHz longitudinal resonance mode with the supplied sonotrode for applications such as cavitation in water-based processes. A modal analysis was performed to assess the resonance frequency during free vibration and investigate the impact of loading on the frequency due to the application. Initially, a convergence study was performed to confirm stability of the resonance mode calculation (Figure 3a); subsequent models utilized approximately 50,000 hex elements. In Figure 3b the FEM-determined resonance modes for various conditions are shown: two longitudinal resonance modes were found at $18<f<21$ kHz at room temperature (RT in Fig. 3b) and service temperature (200°C) (ST in Fig. 3b). By applying a damping condition to the sonotrode, consisting of polymer material, the lower of the longitudinal modes was shifted by approximately +1 kHz.

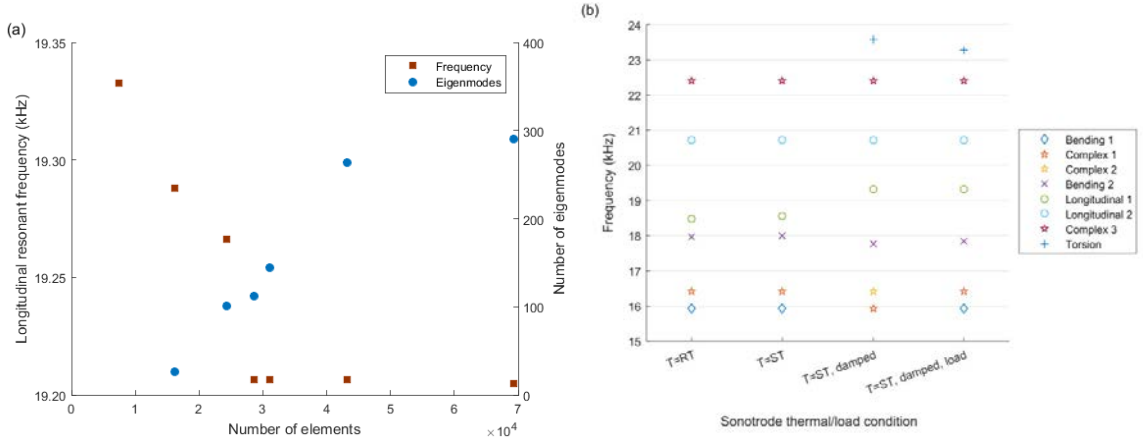

Figure 3. Modal analysis of commercial booster and sonotrode: (a) effect of mesh density on stability of longitudinal resonance mode and number of eigenmodes for 15<*f*<30 kHz (convergence study); (b) resonance modes and respective frequencies under different thermal and load conditions.

3.1.2. Thermal isolation performance

A thermal simulation was performed, which determined that the time to achieve a set point was approximately 10 minutes (Figure 44a). The thermal reference point was located midway between the heating elements. The heater's duty cycle was then scaled back to maintain the set point. An interaction was then introduced at interfaces in contact with the polymer; this applied a thermal boundary condition of 473 K via a surface interaction with a thermal coefficient of 24.5 $W.m^{-2}$. A simulated period of 2 hours did not demonstrate significant thermal rise at the top of the booster; the predicted temperature was approximately 40°C (Figure 44b). Modification of the running conditions to accommodate different test materials will require re-verification of the model.

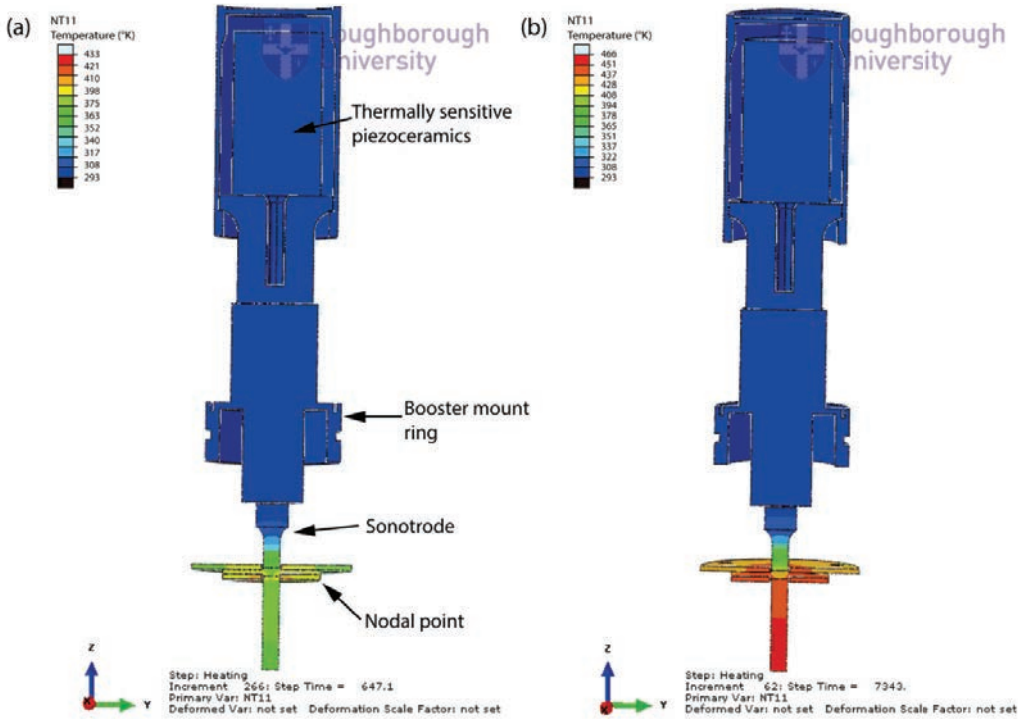

Figure 4. Temperature maps for cross-section of transducer (die not shown): (a) set point at ~10 min; (b) with polymer interaction after ~2 h

3.2. Fluid dynamics of polymer melt

Scaling up any device, in which US interacts with polymer melt, requires understanding of the process. Such interaction may be complex and requires consideration of the sonotrode's resonance mode shape, frequency and amplitude of vibration of the respective surfaces. This is in addition to appropriately modeling the fluid's rheological behavior. There is a large body of literature dealing with the prediction of fluid flow; however, there are relatively few examples considering the flow enhancement of non-Newtonian fluid due to the influence of US. Two such examples form the basis of this work. Lee and Kim (2008) predicted significant flow enhancements of polymer melt by US but the application involved vibration of the entire die by simple sinusoidal movement. Deshpande and Barigou (2001) simulated various materials under the flow of gravity with a vibrating (low frequency) conduit.

The approach considered here simplifies the US parameters: the mode shape is longitudinal with an assumed vibration frequency of approximately 20 kHz (125.66E3 rad/s) and peak-to-peak amplitude of 100 μm. Utilising CFD and FSI in Abaqus produced near identical magnitudes for average outlet velocity for the interstitial die scenario without US; however, they differ in their predicted responses to US. To implement a vibrating sonotrode, the CFD simulation used a velocity (v) boundary condition with amplitude A:

$$v_y = A\omega \sin(\omega t) \tag{4}$$

(where $\omega = 2\pi f$) in addition to a displacement (x) boundary condition:

$$x_y = A\cos(\omega t) \tag{5}$$

with mesh control by arbitrary Lagrangian-Eulerian adaptive meshing. For the pure CFD approach the outlet velocity under US action demonstrated sinusoidal fluctuation at the driving frequency although the time-averaged velocity remained unchanged. The FSI simulation applied Eq. 5 to the displacement of the sonotrode; the CFD co-simulation did not require additional boundary conditions. FSI encountered numerical instability after the boundary-condition change on the sonotrode; fluid flow was also observed around the sonotrode indicating a leak despite the zero-tolerance geometry seal in the model.

CEL simulations were performed as single-element-depth 2D scenarios in order to reduce computation cost. The fluid outlet velocity was in the same order of magnitude compared to that in the CFD analysis. Action of the sonotrode (100 μm p-p; Eq. 5) accelerated fluid flow by an order of magnitude (Figure 55). Due to the relatively slow inlet velocity and default non-coupled contact behavior, the fluid and sonotrode were then subsequently out of contact for thousands of oscillation cycles. Given the high pressures (50-200 MPa) in the injection die and the viscous behavior of the melt, it is believed that separation of the surfaces is unlikely to occur. The stable time increment (dt) required to achieve convergence was approximately 1×10^{-8} s; enforcing a Eulerian-Lagrangian sticky contact behavior to prevent separation of the fluid and sonotrode decreased dt to 1×10^{-14} s. Thus, a CEL approach for a viscous material has a very high resource demand, particularly for the simulation of 3D scenarios.

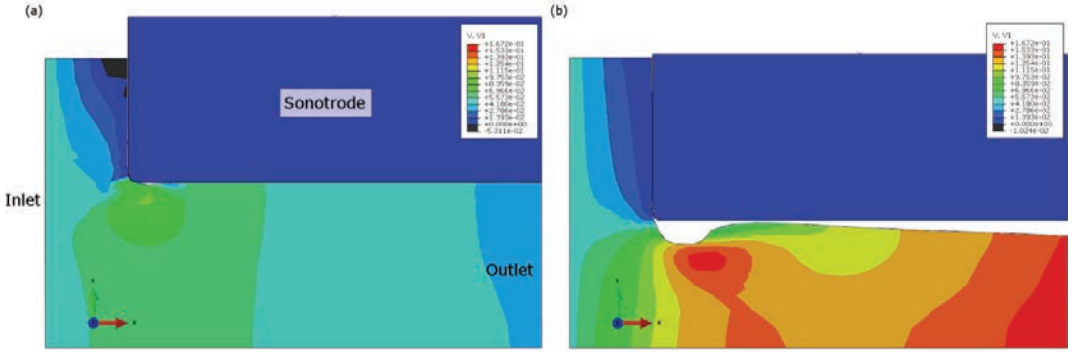

Figure 5. CEL simulation: (a) flow before US, and (b) acceleration of fluid flow due to impact of the sonotrode. The image legend shows the fluid velocity in the x-axis (V1) in units of $m.s^{-1}$.

3.3. Thermally isolated transducer

The design objective of thermally isolating piezoceramics from a hot object was achieved by specifying a machinable ceramic for the sonotrode material. During manufacture it was observed that adding fine features – such as the internal M10 screw thread – made the Macor material vulnerable to damage. Threading was essential for attaching the sonotrode to both transducer and die; however, they are potential crack-initiation sites. Therefore, the sonotrode component was assembled by hand instead of applying a large torque using tools.

In this section simulation results for resonance and thermal performance are presented. The thermal predictions were experimentally validated, and flow enhancement of the prototype device was tested using a dry material.

3.3.1. Structural resonance

Modal analysis by FEM demonstrated 17 vibration modes between 14 and 25 kHz; 2 modes were torsional and the remaining were bending. Using vibrometry, the maximum internal displacement of the die perpendicular to the face was approximately 3.2 μm peak-to-peak at 15.75 kHz (Figure 66a). Bending modes were confirmed by observing radial vibration of the Macor rod (Figure 66b). Torsional vibration was evident at around 17.5 kHz, as predicted by FEM, when the transducer loosened and rotated under US vibration.

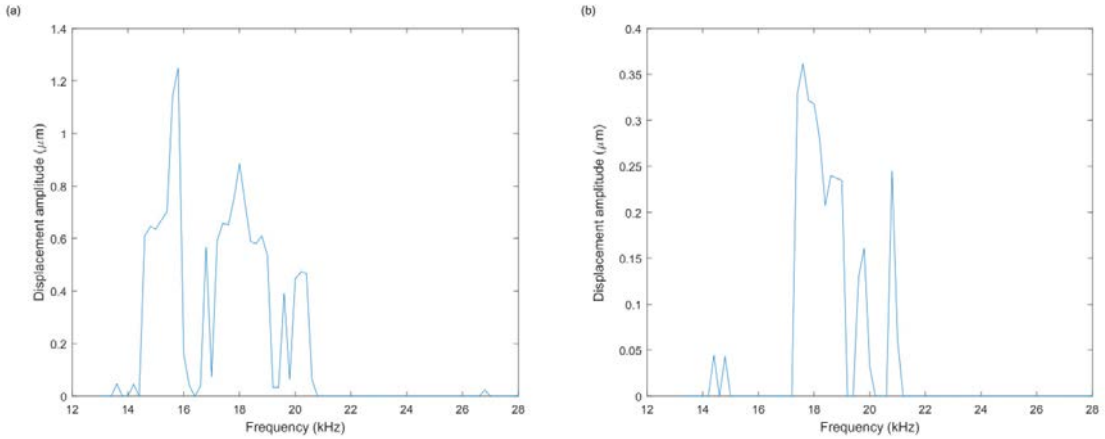

Figure 6. Surface displacement of (a) die internal face (perpendicular) and (b) Macor rod (radial)

3.3.2. Thermal isolation performance

Simulations showed that for an empty die the temperature set point of 150°C was achieved within 70 s, which was confirmed experimentally. Reaching a steady state took approximately 9 minutes. Surface-temperature magnitudes were lower than those predicted by FEM as shown in Table 3, which was due to the omission of thermal losses (radiation, convection) in the simulation. The Macor rod provided full thermal isolation due to its low thermal conductivity and the length of the rod (Figure 77).

Table 3. Macor rod surface temperature versus distance from die.

Distance from die surface (mm)	**Temperature (°C)**	
	FEM	**Experimental**
0	150	125
21	116	80
26	95	60
33	77	50

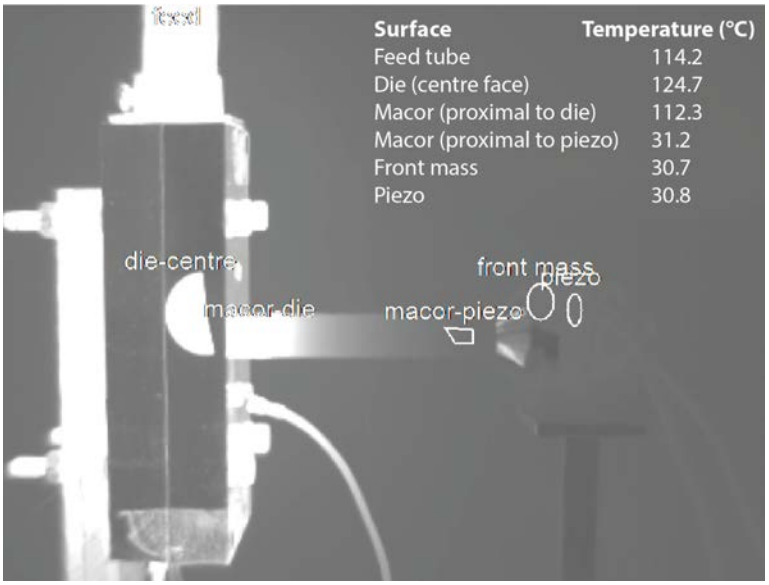

Figure 7. Thermal image of the manufactured device at set point, 150°C. Emissivity stickers were used at each measurement point.

3.3.3. Flow enhancement

Early experimental tests utilized sand as a fluid analogue. The angle of the die was altered as shown in Figure 88 to investigate its effect on the flow rate. At small angles the flow rate was dominated by gravity so applying US had negligible effect. Increasing the angle demonstrated that the US vibration of the die enhanced flow of the sand (Table 4).

Further flow-enhancement experiments using polymer are planned.

Table 4. US-enhanced flow of sand through thermally isolated transducer

	Flow rate ($g.s^{-1}$)		
Die angle α (°)	**US off**	**US on**	**Δ (% ± %)**
17	8.0 ± 0.1	7.9 ± 0.2	0
45	5.4 ± 0.2	5.8 ± 0.2	5.8 ± 0.4
50	4.2 ± 0.1	5.0 ± 0.1	18.6 ± 0.7

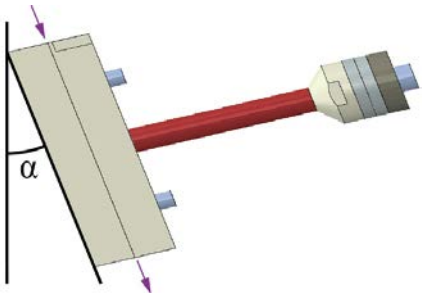

Figure 8. Diagram of experimental setup of thermally isolated transducer showing orientation angle.

4. Conclusions

FEM techniques were employed to confirm the manufacturer's specification for a commercialized titanium sonotrode. Changes in the resonance frequency occurred under the polymer injection molding application but retained the resonance mode indicating that the device is likely to perform as expected. Thermal analysis showed that the piezoceramics are unlikely to be exposed to depolarizing temperatures.

Three approaches were used within Abaqus for fluid dynamics. A pure CFD simulation was unable to demonstrate a flow enhancement but exhibited sinusoidal velocity output. The coupled FSI method encountered numerical issues related to a necessary boundary-condition alteration. The CEL approach had high computational costs, which were related to the viscous material and a need for solving the contact problem. The investigations conclude that CEL is currently impractical; FSI holds promise if the DOF/contact-related issue can be resolved. CFD will be pursued further, since limited examples are available in literature.

Thermal isolation achieved through use of a ceramic sonotrode was demonstrated to be highly effective. The prototype shows promising flow enhancement.

Acknowledgements

The authors acknowledge funding provided by the Innovate UK project ULTRAMELT. The assistance of Robert Balfour with experimental work is gratefully acknowledged.

References

Deshpande, N., Barigou, M., 2001. Vibration flow of non-Newtonian fluids. Chemical Engineering Science 56, 3845-3853.

Ibar, J., 1998. Control of Polymer Properties by Melt Vibration Technology: A Review. Journal of Polymer Engineering and Science 38, 1-20.

Lee, J., Kim, N., 2008. Prediction of charging rate in ultrasonic vibration of injection molding. Journal of Materials Processing Technology 201, 710-715.

Mueller, T., Henning F., 2015. Simulation of combined forming and injection molding processes. 2015 SIMULIA Community Conference

Wang, J., Pengcheng X., Weimin Y., Yumei D., 2009. Online pressure-volume-temperature measurements of polypropylene using a testing mold to simulate the injection-molding process. Journal of Applied Polymer Science 118, 200-208.